https://dx.doi.org/10.22161/ijaers.4.11.6 *ISSN: 2349-6495(P) | 2456-1908(O)*

Some aspects of Cold Deformation studies of Al-ZrB_2 composites

C. Venkatesh[1], B. Chaitanya[2], K S M Yadav[3]

[1,2] Asst.Professor, Dept. of Mechanical Engineering, Ace Engineering college,Ghatkesar, Hyderabad,India.
[3]Research Scholar, Department of Metallurgical and Materials Engineering, NIT Warangal, India

Abstract— *In the present study Al-ZrB_2 composite were made by powder metallurgy route adding different amounts of synthesized ZrB_2 powder (2, 4, 6, 8, 10 wt. %). The ZrB_2 powder was synthesized by using self-propagating high temperature synthesis (SHS). The samples of different aspect ratios (0.35, 0.5 and 0.65) were made and then sintered at 550^{o}C under continuous argon gas atmosphere in a tubular furnace for 1 hour. The microstructure of the composites had shown that there is no chemical adhesion between Al matrix and ZrB_2 reinforcement. Hardness of the composites increased with increase in the amount of ZrB_2 reinforcement. The hardness of the composites increased with increase in amount of ZrB_2 reinforcement. It was found that the formability stress index increased with the increase of preform fractional density and decreased with the aspect ratio. Relation between various stress ratios, axial strain and relative densities were analyzed. Statistical fitting methods are used on the curve drawn between the axial strain and the stress formability index. The compacts of lower aspect ratio and high initial preform density were found to have a very high fracture strain.*

Keywords— Powder metallurgy, ZrB_2, Workability, Relative density, Fracture strain.

I. INTRODUCTION

In some situations Powder metallurgy (P/M) may be the only manufacturing technique which can be used for the production of composite materials, porous materials, refractory materials and high duty special alloys. P/M gives an edge over other manufacturing techniques in cost efficiency, for higher volume production of complicated components. In most cases such components are manufactured using a conventional P/M route which involves deformation of the metal powder followed by sintering [1].

Aluminium metal matrix composites were gaining great scope for applications within aerospace, defense, automotive industries and various other fields [2]. Aluminium MMCs have a great application potential in automotive engineering components i.e, braking systems, piston rods, piston pins, pistons, structural frames, valve spring caps, brake discs, disc brake caliper, brake pads, cardan shaft, engine heads etc. Axle tubes, reinforcements, blade, gear box casing, turbine, fan and compressor blades are some other significant applications in military and civil aviation for Aluminium MMCs. MMCs and alloys are extensively used over metals as they offer higher specific properties (properties/unit weight) of strength, stiffness, higher specific modulus, thermal stability, tribological properties and various other mechanical properties which enhances the product performance [3-4].

Titanium diboride (TiB_2) and zirconium diboride (ZrB_2) are significant boride ceramics which exhibit superior properties like high melting point, extremely high hardness and wear resistance, low specific gravity, magnetic, electrical properties, with high mechanical properties and chemical inertness at elevated temperatures.

In the present study an attempt was made to investigate the deformation behavior of Al-ZrB_2 composites under triaxial stress state conditions. There were few researchers who reported on the deformation behavior of Cu-SiC, Cu-TiC, Al-Cu, Cu-ZrB_2 etc. The ZrB_2 used was synthesized by using self-propagating high temperature synthesis (SHS).

II. EXPERIMENTAL DETAILS

Aluminium:

Aluminium powder (99.99%) was procured from SRL pvt.ltd, Mumbai, India. The particle size of the Al powder is found to be 40µm (-325 mesh size). The particle morphology of aluminum powder was shown Fig. (1a).

https://dx.doi.org/10.22161/ijaers.4.11.6 *ISSN: 2349-6495(P) | 2456-1908(O)*

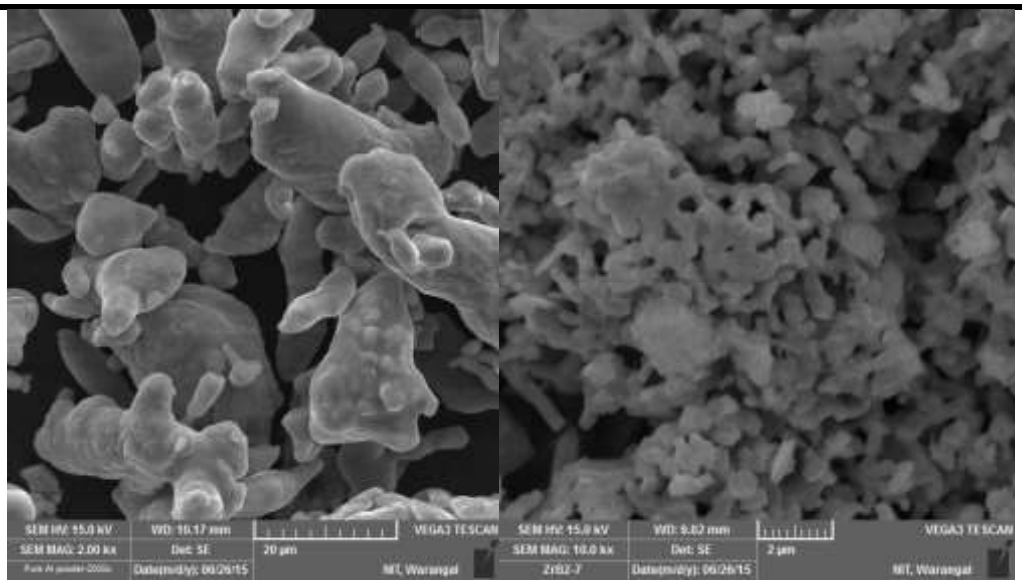

Fig. 1: a) SEM image of Al powder. b) SEM image of ZrB_2 powder

Zirconium Diboride (ZrB_2):

ZrB_2 powder was synthesized by self-propagating high temperature synthesis (SHS) technique with ZrO_2, H_3BO_3 and Mg as raw materials mixed homogeneously in quantities according to stoichiometric equation (1).

$$ZrO_2\ (s) + 2H_3BO_3\ (s) + 5Mg\ (s) \rightarrow ZrB_2\ (s) + MgO\ (s) + 3H_2O\ (g) + \Delta H \quad (1)$$

The 20gm mixture of charge was placed in a stainless steel boat and heated upto 800^0C at a rate of 10^0C/min. The reaction gets initiated at 720^0C. The whole reaction process was carried out in a tubular furnace with continuous supply of argon gas to maintain controlled atmosphere. The reacted mixture was grounded and leached with HCL solution and ZrB_2 powder was tapped [5]. The particle morphology of SHS ZrB_2 powder was shown Fig. (1b).

Compaction:

Compacts of 20mm diameter of pure Al and Al- ZrB_2 (2, 4, 6, 8, 10 wt%)were made in different aspect ratios (L/D) i.e; 0.35, 0.5, 0.65 The variations were achieved by varying powder quantities and compaction loads respectively. A 25Ton manual hydraulic press was used for compaction of powder preforms.

Micro-hardness test:

The surface of the preforms was polished to mirror finish by conventional polishing techniques. Micro-hardness tests were conducted on SCIMADZU micro-hardness tester. 200gm load and 10sec dwell time during loading are the parameters used during micro-hardness tests.

Cold deformation experiments:

The density measurements of preforms were carried out using Archimedes principle. The height and diametric measurements were recorded by digital vernier calipers. All the deformation experiments were carried out on a 50Ton hydraulic press with mirror polished flat dies (top and bottom flatens). A constant ram feed rate of 0.7mm/min was maintained during all the deformation experiments [6]. Extreme care was taken to place the cylindrical specimen within the platens, concentric with the central axis of the hydraulic press (loading direction). Cylindrical preforms were cold upset between flat platens. A set of 6 preforms of same composition were used in incremental loading conditions in order to make a plot for true axial stress and true axial strain. This was because, to determine dimensional measurements and other calculations at different points during loading upto fracture. Axial deformation was continued until a visible crack appeared on the free surfaces of the deforming compacts as shown in Fig 2.

https://dx.doi.org/10.22161/ijaers.4.11.6 *ISSN: 2349-6495(P) | 2456-1908(O)*

Fig. 2: Al composite before and after deformation between the flatens.

Fig. 3: Deformed Al-ZrB_2 composites of different aspect ratios covered with Teflon tape for density measurements.

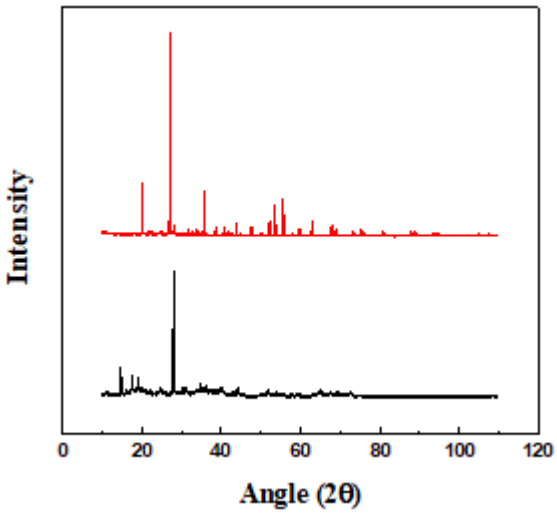

Fig. 4: XRD patterns of Al and ZrB_2 elemental powders.

2.6 Theoretical analysis:

In the upsetting of P/M parts as shown in Fig. (3), the height decreases, the average density increases, and the various stress increases. The expressions for the normal stress *(σ_z)*, normal strain *(ε_z)*, hoop stress *(σ_θ)*, hoop strain *(ε_θ)*, hydrostatic stress *(σ_m)*, effective stress *(σ_{eff})*, and effective strain *(ε_{eff})* are taken from Selvakumar *et al.*[7] and Narayanasamy et al.[8].

Initial diameter- (D_o).

Initial height- (h_o).

Initial preform density (ρ_o).

Contact diameter at the top- (D_{CT}).

Contact diameter at the bottom- (D_{CB}).

Bulged diameter- (D_B).

Height of the preforms- (h_f).

Density of the preforms- (ρ_f).

Using the load, dimensional parameters and density, different true stresses (namely σ_z, $\sigma\theta$, σ_m and σ_{eff}) and different true strains, (namely ε_z and ε_θ) and workability parameters (β_σ).

Triaxial Stress State Condition

$$\alpha = \frac{A}{B} \quad (2)$$

$$A = (2 + R^2)\sigma_\theta - R^2(\sigma_z + 2\sigma_\theta) \quad (3)$$

$$A = (2 + R^2)\sigma_z - R^2(\sigma_z + 2\sigma_\theta) \quad (4)$$

$$\text{Hoop stress, } \sigma_\theta = \left[\frac{2\alpha + R^2}{(2 - R^2 + 2R^2\alpha)}\right]\sigma_z \quad (5)$$

$$\text{Hydrostatic stress, } \sigma_m = \frac{\sigma_z + 2\sigma_\theta}{3} \quad (6)$$

https://dx.doi.org/10.22161/ijaers.4.11.6 *ISSN: 2349-6495(P) | 2456-1908(O)*

Effective stress, $\sigma_{eff} = \left[\frac{\sigma_z^2+2\sigma_\theta^2-R^2(\sigma_\theta^2+2\sigma_z\sigma_\theta)}{2R^2-1}\right]^{0.5}$ (7)

Relative density, $R = \left[\frac{\rho_f}{\rho_{th}}\right]$ (8)

Formability Stress Index, $\beta = \frac{3\sigma_m}{\sigma_{eff}}$ (9)

III. RESULTS AND DISCUSSIONS

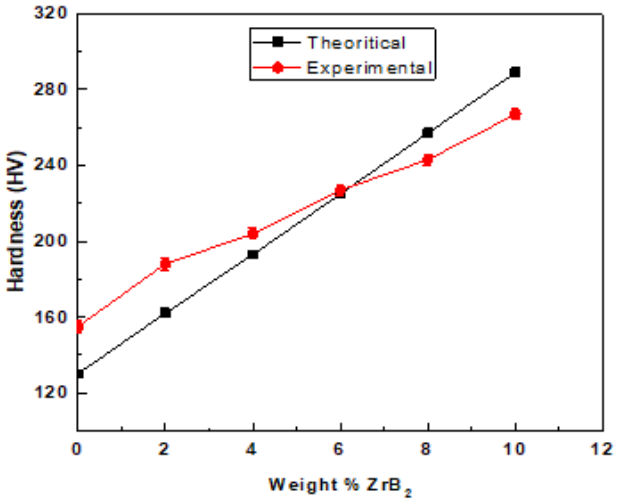

Fig. 5: Hardness of Al - ZrB_2 composites.

The Fig. (5) shows that the experimental micro hardness values of the composites are higher than the theoretical hardness values upto 6% ZrB_2 and then lower than theoretical values because of increased porosity as the ZrB_2 quantity increased in the composites.

The sintered microstructure of pure Al and Al+10% ZrB_2 were as shown in fig. (6). the scanning electron microscope micrographs show that there was no chemical bonding between aluminum and ZrB_2 particles. The porosity increased with the increase in the ZrB_2 reinforcement in the composite. This was because the hard ZrB_2 reinforcement particles inhibiting the transfer of load during compaction which resulted in low relative density. The Fig. (7) shows the microstructure of Al+10% ZrB_2 composite showing the closure of pores due to deformation there by increase in the density.

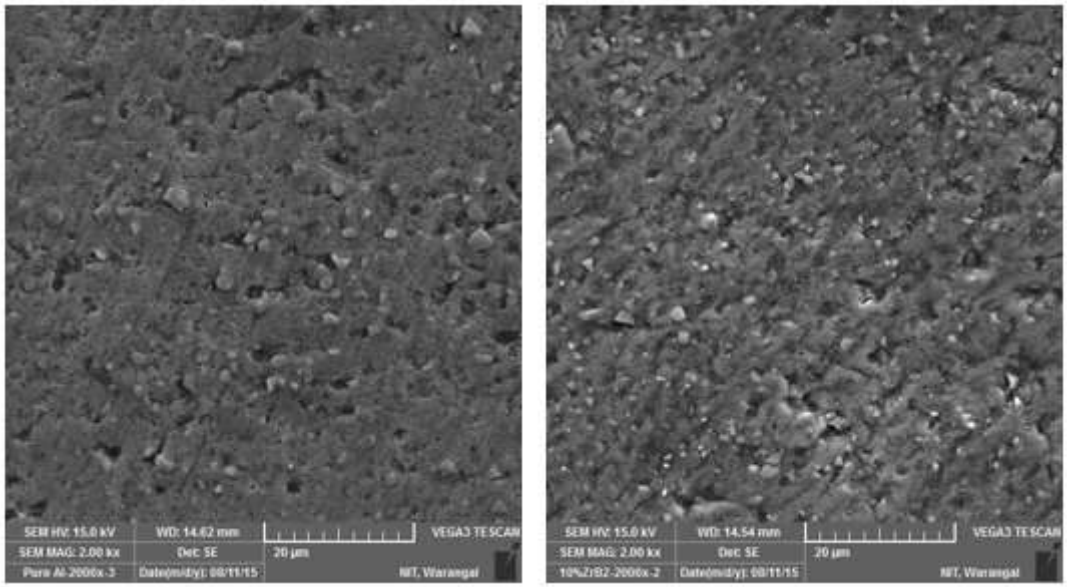

Fig. 6: a) SEM micrograph of pure Al & b) SEM micrograph of Al+10% ZrB_2.

https://dx.doi.org/10.22161/ijaers.4.11.6 *ISSN: 2349-6495(P) | 2456-1908(O)*

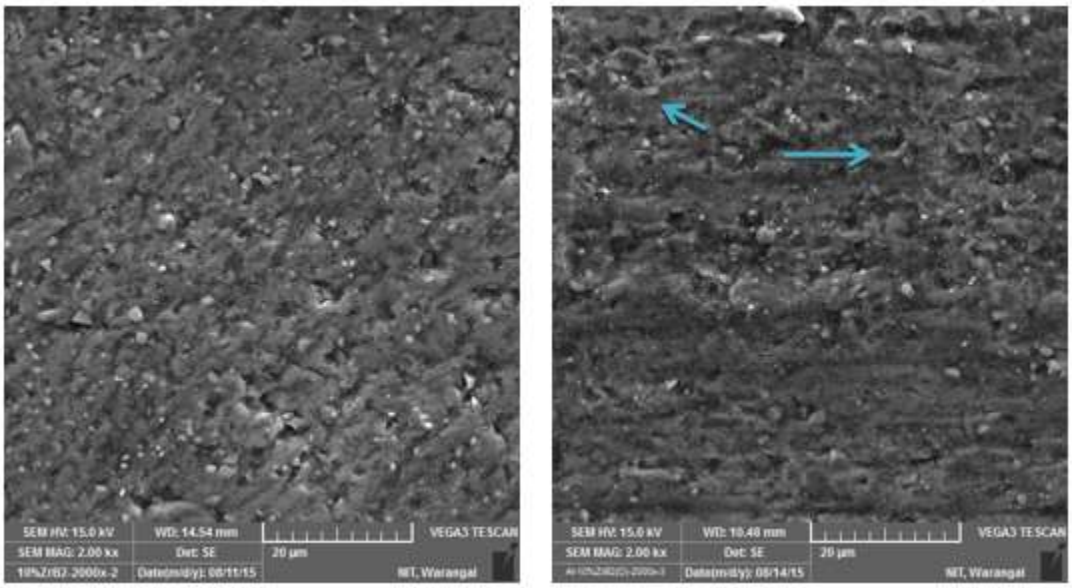

Fig. 7: a) SEM micrograph of Al+10% ZrB_2 before deformation& b) SEM micrograph of Al+10% ZrB_2 after deformation upto fracture

The Fig. (8) Shows the relation between the relative densities attained and the axial strain for the Al-ZrB_2 preforms.

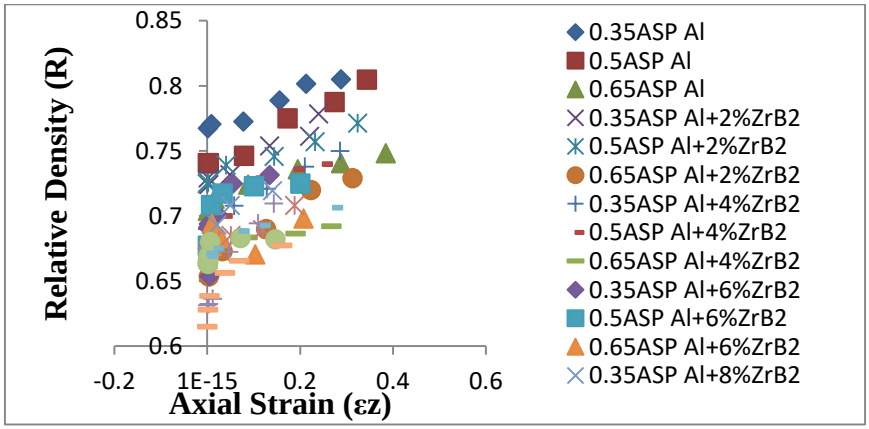

Fig. 8: Relative density(R) Vs Axial strain.

A statistical curve fitting techniques were adopted on the curves of results obtained and the prediction equation developed from the curves was checked for its applicability by comparing the correlation coefficient 'R^2' values. These values can be used for modeling purposes and can also serve as prediction equations. In the present study, two different curve fitting techniques namely power law and parabolic curve fitting were used.

Fig. (9-11) shows the plot drawn between relative density and formability stress index (β). A statistical fit was made using polynomial function and power law function.

https://dx.doi.org/10.22161/ijaers.4.11.6 ISSN: 2349-6495(P) | 2456-1908(O)

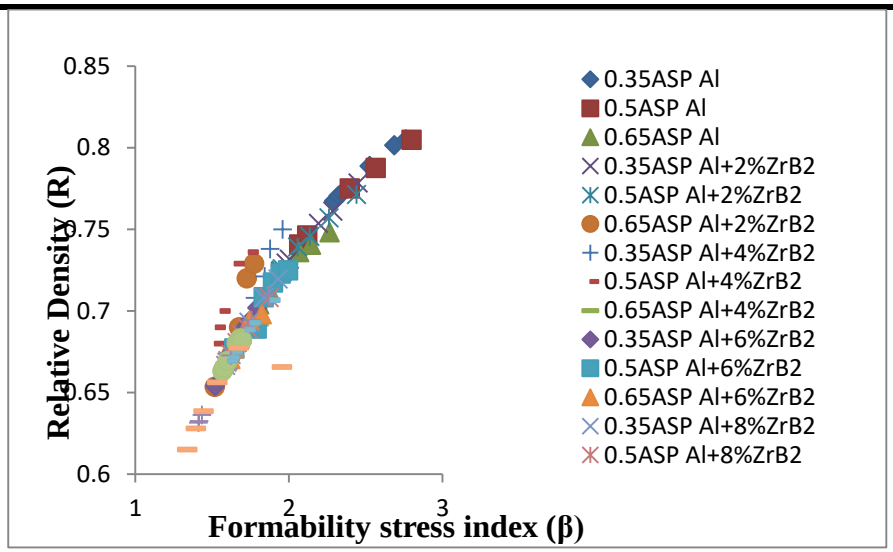

Fig. 8: Relative density (R) Vs Formability stress index (β).

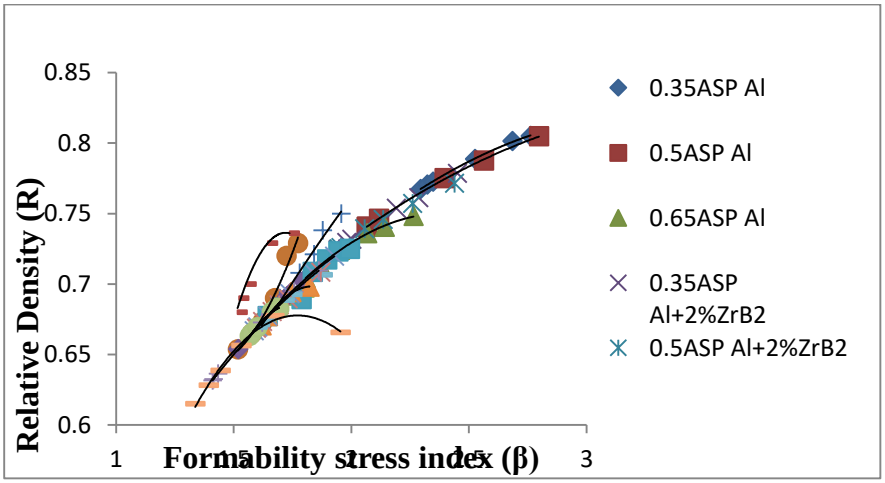

Fig. 9: Relative density (R) Vs Formability stress index (β) (parabolic curve fitting).

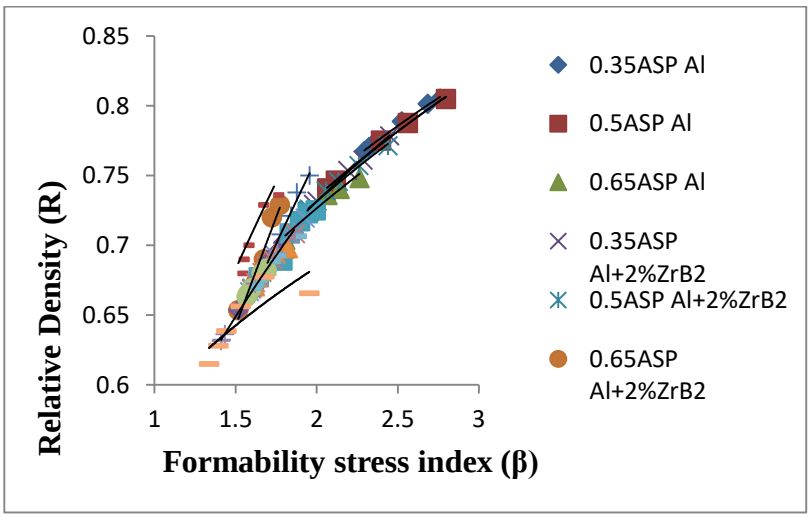

Fig. 10: Relative density (R) Vs Formability stress index (β) (power law curve fitting).

https://dx.doi.org/10.22161/ijaers.4.11.6 *ISSN: 2349-6495(P) | 2456-1908(O)*

Table. 1: Parabolic curve fitting equations and R^2 values of Relative density (R) Vs Formability stress index (β).

Aspect ratio	Sample	Equation	R^2 value
0.35	Pure Al	$y = -0.0517x^2 + 0.3429x + 0.2528$	0.9994
0.5		$y = -0.0369x^2 + 0.2669x + 0.3467$	0.9997
0.65		$y = -0.1281x^2 + 0.6164x + 0.0088$	0.999
0.35	Al+2%ZrB_2	$y = -0.0312x^2 + 0.2423x + 0.3715$	0.9985
0.5		$y = -0.0591x^2 + 0.3528x + 0.2623$	0.9985
0.65		$y = 0.5965x^2 - 1.6489x + 1.7814$	0.9767
0.35	Al+4%ZrB_2	$y = -0.0652x^2 + 0.485x + 0.0522$	0.9819
0.5		$y = -0.9354x^2 + 3.2948x - 2.1615$	0.9876
0.65		$y = -0.3836x^2 + 1.416x - 0.614$	0.9931
0.35	Al+6%ZrB_2	$y = -0.0311x^2 + 0.2797x + 0.3008$	0.9937
0.5		$y = -0.001x^2 + 0.1548x + 0.4239$	0.9393
0.65		$y = -0.6005x^2 + 2.2015x - 1.3196$	0.9975
0.35	Al+8%ZrB_2	$y = -0.1078x^2 + 0.5343x + 0.0905$	0.9999
0.5		$y = -0.1123x^2 + 0.5328x + 0.1045$	0.9987
0.65		$y = -0.5879x^2 + 2.0782x - 1.1503$	0.9946
0.35	Al+10%ZrB_2	$y = -0.0901x^2 + 0.4676x + 0.1515$	1
0.5		$y = -0.1924x^2 + 0.8034x - 0.1235$	0.9999
0.65		$y = -0.3428x^2 + 1.2145x - 0.398$	0.9911

From the Fig. (12-13) it was found that the relative density increases as the stress ratio parameter increases.

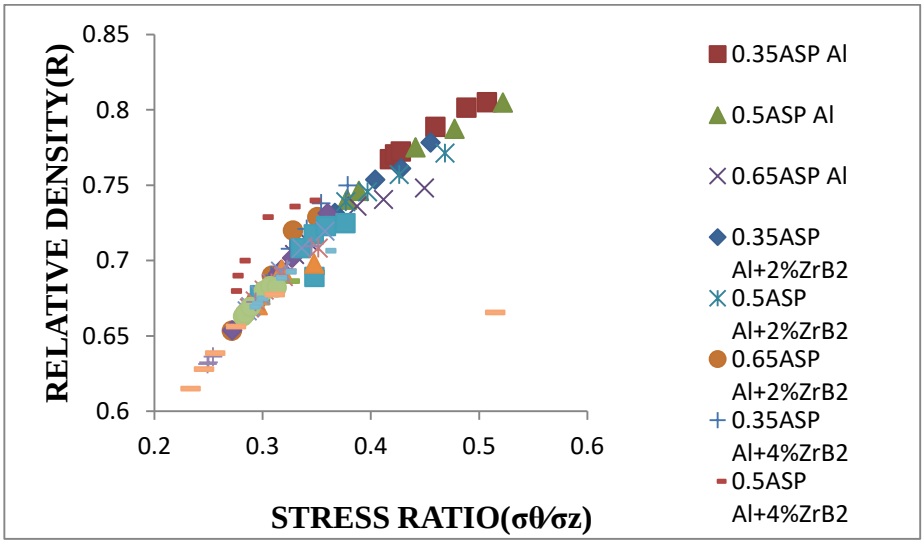

Fig. 11: Relative density Vs Stress ratio(σθ/σz).

https://dx.doi.org/10.22161/ijaers.4.11.6 ISSN: 2349-6495(P) | 2456-1908(O)

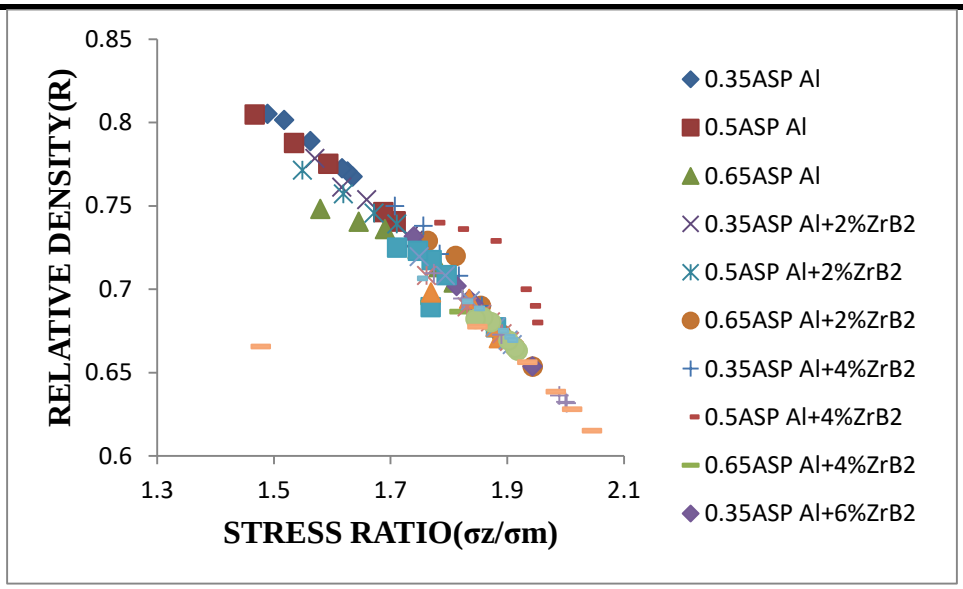

Fig. 12: Relative density Vs Stress ratio(σz/σm).

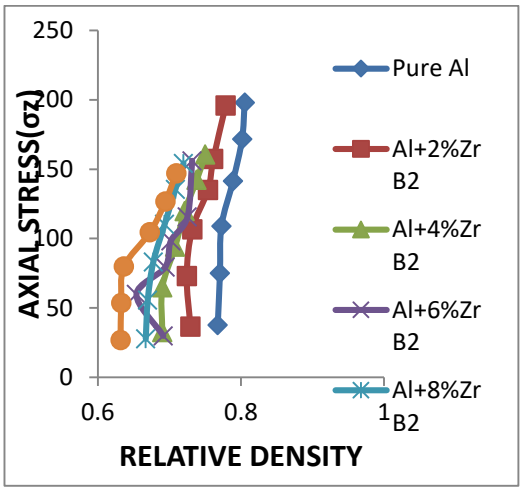

(a)

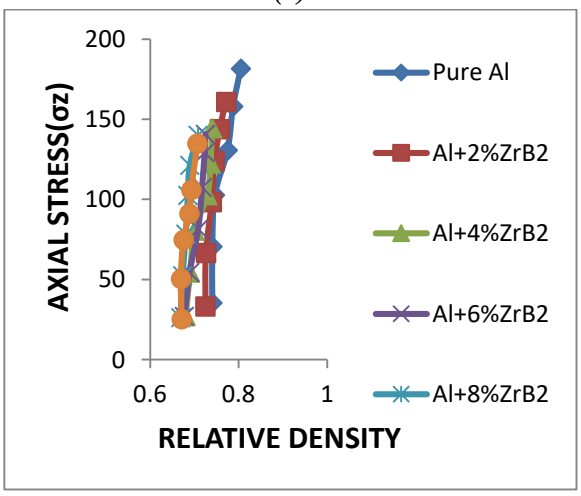

(b)

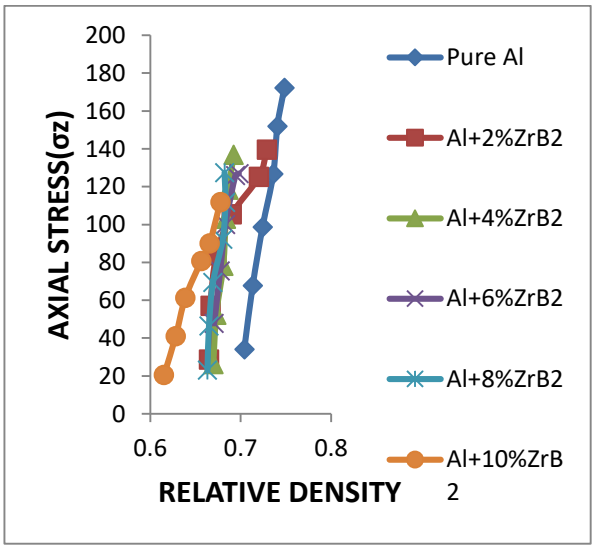

(c)

Fig. 15: Axial stress (σ_z) Vs Relative density (R) (a) 0.35 ASPR, (b) 0. 5 ASPR and (c) 0.65 ASPR

The Fig. 15(a-c) shows the plot of axial stress (σz) against the relative density R. The experiment has been done with preforms with initial densities ranging from 0.6 to 0.75 and aspect ratios ranging from 0.35 to 0.65. Along with the densification, the load bearing capability of the preforms also increase, as is evident from the higher stress values in the plot 15(a-c)

It was found that the preform with 10 % ZrB_2 and 0.35 aspect ratio had densified more. Preforms with high initial preform density had higher load bearing capacity and longer

https://dx.doi.org/10.22161/ijaers.4.11.6 *ISSN: 2349-6495(P) | 2456-1908(O)*

strain to failure. This was due to the presence of lesser number of pores.

IV. CONCLUSIONS

- The porosity increased with increased quantity of ZrB_2 reinforcement, as the ultra-hard ZrB_2 particles in the composite don't allow the load applied while compaction to close the pores.
- The hardness of the composites increased with increased amount of ZrB_2 reinforcement in the composite.
- The formability behaviors of sintered Al-ZrB_2 composite preforms had been studied in this paper. The formability stress index increased with increase in initial preform fractional density and decreases with the aspect ratios. A statistical fitting methods were to draw curves between the relative density and axial strain, axial strain and the formability stress index. The parabolic curve fitting was found to give better prediction results. The initiation of crack appeared at a very high fracture strain for the compacts with higher value of the aspect ratio and high initial preform density.

REFERENCES

[1] J. Mascarenhas, Powder metallurgy: a major partner of the sustainable development, Materials Science Forum, 455- 456 (2004), 857–860, doi: 10.4028/ www.scientific.net/ MSF.455-456.857.

[2] Dieter GE, Mechanical Metallurgy, New York: McGraw-Hill 3rd ed., 1981.

[3] A. Riaz Ahamed , P. Asokan and S. Aravindan, EDM of hybrid Al–SiCp–B4Cp and Al–SiCp–Glassp MMCs, Journal Advance Manufacturing Technol (2009) 44:520–528. DOI 10.1007/s00170-008-1839-0.

[4] M. Ramulu, G. Paul and J. Patel, EDM surface effects on the fatigue strength of a 15vol% SiC_P/Al metal matrix composite material, Composite structures 54 (2001) 79-86.

[5] Sumathi, M., Selvakumar, N., & Narayanasamy, R., Workability studies on sintered Cu-10SiC preforms during cold axial upsetting, Materials and Design, 39 (2012), 1–8, doi: 10.1016/j.matdes.2012.02.004

[6] Narayanasamy, R., Anandakrishnan, V., & Pandey, K. S., Effect of carbon content on workability of powder metallurgy steels, Materials Science and Engineering A, 494 (2008), 337–342, doi:10.1016/j.msea.2008.04.022

[7] Selvakumar N and Narayanasamy R., Phenomenon of strain hardening behaviour of sintered aluminium preforms during cold axial forming, Journal of Materials Processing Technology, 142 (2003), 347-354, doi:10.1016/S0924-0136(03)00605-8

[8] Harsh Saini, Irfan Khan, Sushil Kumar, Sahil Kumar(2017).Optimization of Material Removal Rate of WEDM Process on Mild Steel Using Molybdenum Wire. International Journal of Advanced Engineering, Management and Science (ISSN: 2454-1311), 3(10), 1001-1005. http://dx.doi.org/10.24001/ijaems.3.10.5

[9] Narayanasamy R, Ramesh T and Pandey KS., Some aspects on workability of aluminium–iron powder metallurgy composite during cold upsetting, Materials Science and Engineering, A391 (2005), 418–426, doi: 10.1016/j.msea.2004.09.018